Experimental and theoretical investigations of the reactions $NH(X\,^3\Sigma^-)+D(^2S)\rightarrow ND(X\,^3\Sigma^-)+H(^2S)$ and $NH(X\,^3\Sigma^-)+D(^2S)\rightarrow N(^4S)+HD(X\,^1\Sigma_g^+)$

Z.-W. Qu, H. Zhu, and R. Schinke[a)]
Max-Planck-Institut für Dynamik und Selbstorganisation, D-37073 Göttingen, Germany

L. Adam and W. Hack
Max-Planck-Institut für biophysikalische Chemie, D-37077 Göttingen, Germany

(Received 11 February 2005; accepted 9 March 2005; published online 24 May 2005)

The rate coefficient of the reaction $NH(X\,^3\Sigma^-)+D(^2S)\xrightarrow{k_1}$products (1) is determined in a quasistatic laser-flash photolysis, laser-induced fluorescence system at low pressures. The NH(X) radicals are produced by quenching of NH($a\,^1\Delta$) (obtained in the photolysis of HN_3) with Xe and the D atoms are generated in a D_2/He microwave discharge. The NH(X) concentration profile is measured in the presence of a large excess of D atoms. The room-temperature rate coefficient is determined to be $k_1=(3.9\pm1.5)\times10^{13}$ cm^3 mol^{-1} s^{-1}. The rate coefficient k_1 is the sum of the two rate coefficients, k_{1a} and k_{1b}, which correspond to the reactions $NH(X\,^3\Sigma^-)+D(^2S)\xrightarrow{k_{1a}}ND(X\,^3\Sigma^-)+H(^2S)$ (1a) and $NH(X\,^3\Sigma^-)+D(^2S)\xrightarrow{k_{1b}}N(^4S)+HD(X\,^1\Sigma_g^+)$ (1b), respectively. The first reaction proceeds via the $^2A''$ ground state of NH_2 whereas the second one proceeds in the $^4A''$ state. A global potential energy surface is constructed for the $^2A''$ state using the internally contracted multireference configuration interaction method and the augmented correlation consistent polarized valence quadrupte zeta atomic basis. This potential energy surface is used in classical trajectory calculations to determine k_{1a}. Similar trajectory calculations are performed for reaction (1b) employing a previously calculated potential for the $^4A''$ state. The calculated room-temperature rate coefficient is $k_1=4.1\times10^{13}$ cm^3 mol^{-1} s^{-1} with $k_{1a}=4.0\times10^{13}$ cm^3 mol^{-1} s^{-1} and $k_{1b}=9.1\times10^{11}$ cm^3 mol^{-1} s^{-1}. The theoretically determined k_1 shows a very weak positive temperature dependence in the range $250\leqslant T/\mathrm{K}\leqslant1000$. Despite the deep potential well, the exchange reaction on the $^2A''$ ground-state potential energy surface is not statistical. © *2005 American Institute of Physics*.
[DOI: 10.1063/1.1899563]

I. INTRODUCTION

NH_i ($i=1,2$) radicals are of great importance for understanding the nitrogen chemistry in flames.[1,2] The amino radical NH_2 is essential in nitrogen flame chemistry such as its isoelectronic counterparts OH and CH_3 in combustion chemistry. In the present investigation, experimental information on the association-dissociation reaction of $NH_2(\tilde{X})$ is obtained via a detour, namely, the reaction of ground-state NH radicals with D atoms.

$$NH(X\,^3\Sigma^-)+D(^2S)\xrightarrow{k_1}\text{products}. \tag{1}$$

The complementary reaction with hydrogen atoms, i.e.,

$$NH(X\,^3\Sigma^-)+H(^2S)\xrightarrow{k_2}\text{products}, \tag{2}$$

which has been studied experimentally and theoretically in Ref. 3 (hereafter termed paper I), provides information only on the production of N(^4S) atoms. Reaction (2) proceeds on the potential energy surface (PES) of the quartet state $^4A''$ ($^4\Sigma^-$ in linear N–H–H configuration; Fig. 1) with a measured rate coefficient $k_2(298\ \mathrm{K})=1.9\times10^{12}$ cm^3 mol^{-1} s^{-1}. The reaction on the doublet PES, $^2A''$, leading to $NH_2(\tilde{X})^{\ddagger}$ cannot be observed in reaction (2), because the initially formed complex decomposes to the educts $NH(X\,^3\Sigma^-)$ and $H(^2S)$.

The pathway via the $NH_2(\tilde{X})$, respectively, $NHD(\tilde{X})$ ground state can be investigated, however, via reaction (1). It encompasses two different reaction paths that both lead to a depletion of $NH(X\,^3\Sigma^-)$:

$$NH(X\,^3\Sigma^-)+D(^2S)\xrightarrow{k_{1a}}ND(X\,^3\Sigma^-)+H(^2S), \tag{1a}$$

$$NH(X\,^3\Sigma^-)+D(^2S)\xrightarrow{k_{1b}}N(^4S)+HD(X\,^1\Sigma_g^+). \tag{1b}$$

The $N(^2D)+HD(X\,^1\Sigma_g^+)$ channel is not accessible at the temperatures considered in this work. The first reaction proceeds on the $^2A''$ PES while the second one occurs on the $^4A''$ PES. If Renner–Teller (RT) coupling between the $\tilde{X}^2A''$ and $\tilde{A}^2A'$ states is ignored, each reaction can be considered as a one-state problem. Reaction (1a) is expected to be much faster than reaction (1b), because the $^2A''$ PES is rather attractive and the reaction is not constrained to near-linear approaches

a)Electronic mail: rschink@gwdg.de

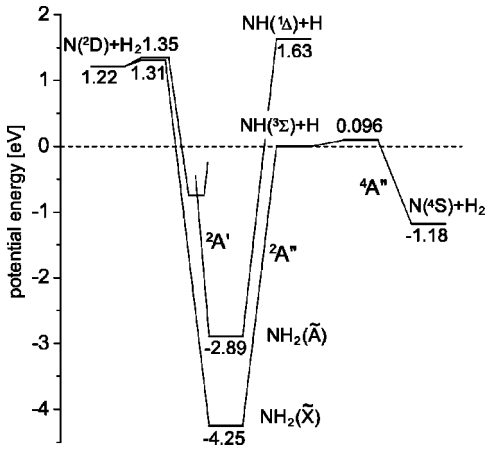

FIG. 1. Schematic energy level and correlation diagram for the reaction $NH(X\,^3\Sigma^-)+H(^2S)\rightarrow$ products. The energies and transition state geometries are the ones calculated in this work (aug-cc-pvqz atomic basis). The conical intersection of the $^2A'$ state with a higher state of the same symmetry is indicated; for a more complete representation, see Ref. 29.

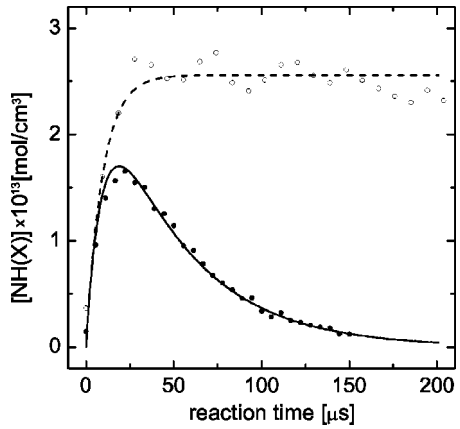

FIG. 2. Typical NH(X) concentration profiles in the absence (○) and presence (●) of D atoms.

as it is on the $^4A''$ PES. Consequently, k_1 is expected to be considerably larger than k_2. Reaction (1) has not yet been studied directly, neither experimentally nor theoretically.

In the present work we measure the rate coefficient for reaction (1) at room temperature via the depletion of NH(X) radicals (Sec. II). We construct a global PES for the $^2A''$ state by electronic structure calculations (Sec. III) and perform classical trajectory calculations on this PES in order to determine k_{1a} (Sec. IV). The rate coefficient k_{1b} is evaluated by trajectory calculations using the $^4A''$ PES constructed in paper I. The conclusions which can be drawn from the joint experimental and theoretical studies are given in Sec. V.

II. EXPERIMENTAL RESULTS

The experiment is performed, as described in paper I, in a quasistatic laser-flash photolysis/laser-induced fluorescence (LIF) system, where "quasistatic" means that the flow through the reaction cell is negligible between the pump and the probe pulses, but sufficient to exchange the gas volume between two subsequent pump pulses. The carrier gas is He at a total pressure of $6.9\ \text{mbar} \leqslant p \leqslant 14.2\ \text{mbar}$.

The experimental setup is described in paper I and in detail elsewhere,[4] thus only the keywords are given here. For the photolysis a XeCl-exciplex laser with pulse energies in the range of 200–400 mJ and a beam area of about 1.1 cm^2 is used. The probe laser is a dye laser with a beam area of 7 mm^2. It is pumped by an exciplex laser.

The NH(X) radicals are obtained by quenching NH($a\,^1\Delta$) with Xe and the NH(a) radicals are produced by HN_3 photolysis. The D atoms are generated in a sidearm of the reactor in a microwave discharge of a D_2/He mixture (0.02–0.03 molfraction D_2 in He). The absolute initial D atom concentration is determined via titration with NO_2. The increase of OD with increasing NO_2 is observed by LIF via the $Q_1(2)$ line of the transition $A\,^2\Sigma^+,\ v=0\leftarrow X\,^2\Pi,\ v=0$ at $\lambda = 307.54$ nm with a dye laser pumped by a Nd:YAG (yttrium aluminum garnet) laser. $NH(X, v=0)$ is detected by exciting the $P_2(2)$ line at $\lambda = 336.48$ nm of the transition $A\,^3\Pi,\ v'=0\leftarrow X\,^3\Sigma,\ v''=0$. The undispersed fluorescence from the excited state is observed in the wavelength range of 335–337 nm perpendicular to the laser beam.

The HN_3 and Xe are added to the reactor via an inner probe which ends about 1 cm above the photolysis volume. The NO_2 for the titration is also added to the system through this probe. Gases with the highest commercially available purity are used: He, 99.9999%, Praxair; Xe, 99.998%, Messer-Griesheim; N_2, 99.995%, UCAR; D_2, 99.7% (rest H_2), Messer-Griesheim; and NO_2, 99.5%, Merck. HN_3 is synthesized by melting stearic acid, $CH_3(CH_2)_{16}COOH$ (97%, Merck), with NaN_3 (99.0%, Merck).

The NH(X) radicals are produced in the fast quenching reaction[4]

$$NH(a\,^1\Delta) + Xe \xrightarrow{k_q} NH(X\,^3\Sigma^-) + Xe. \qquad (3)$$

Typical NH(X) concentration profiles in the absence and in the presence of D atoms are shown in Fig. 2. NH(a) is formed at $t=0$ by the photolysis pulse. In both cases (with or without D atoms present), the NH(X) concentration increases very rapidly in time due to the quenching of NH(a) by Xe. In the absence of D atoms (discharge off, open circles in Fig. 2) the NH(X) concentration stays constant after about $12 \leqslant t/\mu s \leqslant 23$ (depending on the Xe concentration) for more than 300 μs. This means that neither diffusion nor the other gases present in the system (D_2 and HN_3) contribute to the NH(X) consumption (as expected from the rates and concentrations of these molecules). For the individual experiments the Xe concentration is in the range $0.9 \leqslant [Xe]/10^{-8}\ \text{mol cm}^{-3} \leqslant 1.9$, as given in Table I. The dashed line in Fig. 2 is obtained from a simple simulation of the system assuming an initial NH(a) concentration of $[NH(a)]_0 = 2.6\times10^{-13}\ \text{mol cm}^{-3}$ estimated from the HN_3 absorption at the photolysis wavelength and a dissociation quantum yield of one. The subsequent analysis of the NH(X) profiles to determine k_1 start at about $t > 12$ μs depending on the particular experimental conditions.

The NH(X) concentration profile in Fig. 2 in the presence of D atoms (full dots) shows a depletion which is due to reaction (1). The line is the result of a simulation including reaction (1). The D atom concentration is large compared to

TABLE I. Experimental data for the 21 independent experiments.

p (mbar)	$[Xe]\times10^8$ mol/cm^3	$[D_2]\times10^8$ mol/cm^3	$[HN_3]\times10^{11}$ mol/cm^3	$[D]\times10^{10}$ mol/cm^3	k_{eff} (s^{-1})	$k_1\times10^{-13}$ cm^3/mol s
6.9	0.9	1.0	5.2	3.7	12 600	3.4
6.9	0.9	1.0	5.2	3.7	13 600	3.7
6.9	0.9	1.0	5.2	3.7	15 600	4.2
9.8	1.4	0.83	2.6	3.9	19 400	5.0
10.1	1.8	1.1	2.6	5.0	38 700	7.7
10.2	1.7	1.0	2.6	5.0	21 100	4.2
10.3	1.8	1.1	2.6	5.5	29 000	5.3
10.3	1.8	1.1	2.6	5.5	30 000	5.5
10.1	1.9	1.4	2.6	5.9	27 700	4.7
14.2	1.8	2.0	6.5	7.0	20 800	3.0
14.2	1.8	2.0	6.5	7.0	22 000	3.1
14.2	1.8	2.0	6.5	7.0	22 300	3.2
9.8	1.9	1.4	2.6	7.1	27 800	3.9
10.1	1.9	1.4	2.6	7.1	23 000	3.2
10.1	1.9	1.4	2.6	7.1	23 800	3.4
10.1	1.9	1.4	2.6	7.1	24 600	3.5
10.1	1.9	1.4	2.6	7.5	21 700	2.9
10.1	1.9	1.4	2.6	7.5	21 300	2.8
10.1	1.9	1.4	2.6	7.6	33 100	4.4
10.1	1.9	1.4	2.6	7.6	34 300	4.5
10.1	1.9	1.4	2.6	9.0	33 600	3.7

$[NH(X)]_0$ [i.e., the NH(X) concentration at a time $t>20$ μs] and thus pseudo-first-order conditions are realized. From the slope of $\ln[NH(X)]$ versus time first-order rate coefficients k_{eff} are determined by

$$\frac{d\ln[NH(X)]}{dt}=k_{eff}\,[D]. \tag{4}$$

This k_{eff} is converted with the measured D atom concentrations into the second-order rate coefficients k_1.

The results for the 21 independent experiments are summarized in Table I. It is not possible to vary the D atom concentration over a wide range (a factor of 2.4 was realized) and therefore the dependence of the first-order rate coefficient versus [D] cannot be investigated. For the fifth experiment in Table I a rate coefficient is obtained which is much larger than those deduced from the other experiments. We surmise that in this particular experiment the discharge efficiency changed between the measurements of the decay of $[NH(X)]$ and the titration. Therefore, several other experiments were done repeating the kinetic measurement before and after the titration. These results appear in Table I with two or three k_{eff} values and otherwise identical experimental parameters. No significant change was observed in all cases. Nevertheless, the particular value $k_1=7.7\times10^{13}$ cm^3 mol^{-1} s^{-1} was omitted when the average rate coefficient was calculated. The final rate coefficient, obtained as the average of the other 20 measurements, is $k_1(298\ \mathrm{K})=(3.9\pm1.5)\times10^{13}$ cm^3 mol^{-1} s^{-1}. In the small pressure range a pressure dependence of k_1 cannot be observed. The large uncertainty is mainly due to the titration of the D atoms. It takes into account the change of the efficiency of the discharge as described above. This rate coefficient mainly corresponds to reaction (1a), which is exothermic with $\Delta_R H=-1.2$ kcal/mol. The formation of N(^4S) atoms via reaction (1b) is about one order of magnitude slower and thus contributes less than 5% to the overall NH(X) consumption.

III. POTENTIAL ENERGY SURFACES OF $NH_2(\tilde{X}\,^2A'')$ AND $NH_2(\tilde{A}\,^2A')$

In this section we describe the electronic structure calculations for the two lowest states of NH_2: the ground state $\tilde{X}\,^2A''$ and the first excited state $\tilde{A}\,^2A'$ (see Fig. 1). Only the ground state is relevant for the present study. However, the $\tilde{X}\,^2A''$ and $\tilde{A}\,^2A'$ states form a RT pair,[5–7] i.e., they are degenerate for linear geometries, and therefore it is reasonable to consider them together. The first excited electronic state is required for studying the depletion of NH in the first excited state, $a\,^1\Delta$, in collisions with hydrogen atoms.[8] Global PESs for the $\tilde{X}\,^2A''$ and $\tilde{A}\,^2A'$ states of NH_2 have been previously calculated by Pederson *et al.*[9,10] and Ho *et al.*[11] These PESs have been used in several classical[9–13] and quantum-mechanical calculations.[14–16] In what follows R_1, R_2, and α are the two N–H bond distances and the H–N–H bond angle, respectively. Occasionally we also use the Jacobi coordinates appropriate for the $N+H_2$ channel: R, the distance from N to the center of mass of H_2; r, the H_2 bond distance; and γ, the angle between the vectors **R** and **r**. If not stated otherwise, energy is normalized such that $E=0$ corresponds to $NH(X\,^3\Sigma^-)+H(^2S)$ with NH at equilibrium.

A. Electronic structure calculations

The electronic structure calculations for the $\tilde{X}\,^2A''$ and $\tilde{A}\,^2A'$ states are performed on the same level of theory, as described in paper I for the $^4A''$ state. The internally con-

TABLE II. N–H bond distances (in a_0), bond angle α (in degrees), and energies E (in kcal/mol) of the global equilibrium of the $^2A''$ and $^2A'$ states.

	$\tilde{X}\,^2A''$			$\tilde{A}\,^2A'$		
Basis	E[a]	R_{NH}	α	E[a]	R_{NH}	α
aug-cc-pvtz	−96.7	1.947	102.49	−65.08	1.887	145.04
	−97.5[b]	1.94[b]	102.7[b]	64.1[c]	1.88[c]	142.7[c]
aug-cc-pvqz	−97.99	1.943	102.60	−66.68	1.884	145.14
aug-cc-pv5z	−98.35	1.942	102.63	−67.11	1.883	145.15
aug-cc-pv6z	−98.48	1.942	102.68	−67.28	1.883	145.15
Expt.	−98.77[d]	1.936[e]	103.34[e]	−67.18[d]	1.897[f]	144.0[f]

[a]Energies with respect to NH($X\,^3\Sigma^-$)+H(^2S) with NH at equilibrium.
[b]From Table I of Pederson *et al.*, Ref. 10.
[c]From Table I of Pederson *et al.*, Ref. 10; results without Davidson correction.
[d]See the text for details.
[e]Reference 24.
[f]Reference 25.

tracted multireference configuration interaction (MRCI) method[17,18] is used. In order to approximately account for higher excitations and size consistency the Davidson correction is applied.[19] The MRCI calculations are based on optimized full-valence complete-active space self-consistent-field (CASSCF) orbitals.[20,21] If not stated otherwise, the augmented correlation consistent polarized valence quadruple zeta (aug-cc-pvqz) atomic basis set of Dunning[22] is employed. The 1*s* orbital of nitrogen is fully optimized in the CASSCF calculations but frozen in the subsequent CI calculations. There are 45/81 reference configurations with 95/115 reference configuration state functions for the $^2A''/^2A'$ state leading to 275 346/283 405 contracted configurations in the CI calculations. All calculations are performed in C_s symmetry using the MOLPRO suit of programs.[23] The present electronic structure calculations are very similar to those of Pederson *et al.*[9,10] with the exception that the atomic basis is larger, i.e., aug-cc-pvqz compared to augmented correlation consistent polarized valence triple zeta (aug-cc-pvtz).

In order to assess the accuracy of the present study we first calculate, using several basis sets, the critical points on the two PESs by full optimization. The equilibrium geometries and energies of the global minimum of the $^2A''$ and $^2A'$ states are given in Table II. The convergence with respect to the atomic basis size is very fast; the results obtained for the aug-cc-pvqz basis set do not differ much from the results for the augmented correlation consistent polarized valence sextuple zeta (aug-cc-pv6z) basis. The present results agree well with the results of Pederson *et al.*[9,10] obtained with the aug-cc-pvtz basis. The calculated equilibrium coordinates also agree well with the experimental data.[24,25] The energy of the ground-state minimum with respect to NH(X)+H is calculated using thermodynamical data[26,27] and the calculated zero-point energies for $NH_2(\tilde{X})$ (0.519 eV) and NH(X) (0.212 eV). The experimental value of −98.77 kcal/mol agrees well with the calculated value of −98.48 kcal/mol with the large aug-cc-pv6z basis set. The experimental energy of the minimum of the excited state with respect to NH(X)+H is calculated by using the barriers to linearity of the $\tilde{X}\,^2A''$ (11 914 cm^{-1}) and the $\tilde{A}\,^2A'$ (863 cm^{-1}) states as determined by Gabriel *et al.*[7] (Table 3); the two PESs in Ref. 7 have been constructed in a least-squares procedure to exactly reproduce the measured rovibronic transition energies and therefore can be considered as accurate. The calculated value of −67.28 kcal/mol agrees well with the experimental value of −67.18 kcal/mol.

The data for the three asymptotic channels are given in Table III and compared with recent theoretical and experimental data. Again, the results converge fast with the basis size and the agreement with the results of Pederson *et al.*[9,10]

TABLE III. Equilibrium bond distances (in a_0) and energies E (in kcal/mol) for the three different product channels and several basis sets.

	N(^2D)+H_2		NH(X)+H		NH(a)+H	
Basis	E[a]	R_{H_2}	E	R_{NH}	E	R_{NH}
aug-cc-pvtz	28.36	1.404	0.0	1.967	38.30	1.981
	28.9[b]	1.40[b]	0.0	1.97[b]	37.7[c]	1.96[c]
aug-cc-pvqz	28.03	1.402	0.0	1.963	37.54	1.977
aug-cc-pv5z	27.87	1.401	0.0	1.961	37.30	1.976
aug-cc-pv6z	27.80	1.401	0.0	1.961	37.20	1.976
Expt.	30.3[d]	1.401[e]	0.0	1.958[e]	35.9[d]	1.954[e]

[a]Energies with respect to NH(X)+H.
[b]From Table II of Pederson *et al.*, Ref. 9.
[c]From Table I of Pederson *et al.*, Ref. 10; without Davidson correction.
[d]See text for details.
[e]Reference 27.

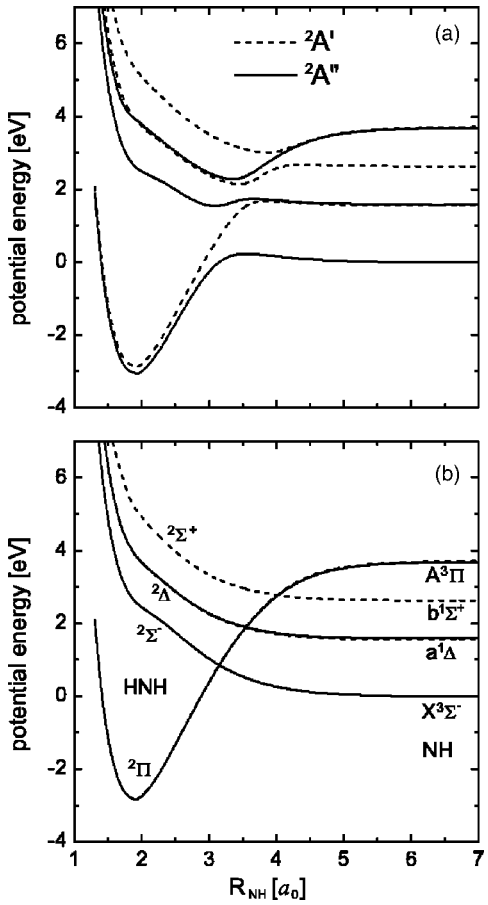

FIG. 3. Cuts through the potential energy surfaces of the lowest six doublet states of NH_2 for bond angles $\alpha=160°$ (a) and $\alpha=180°$ (b). The other H–N bond length is $1.943a_0$ and the aug-cc-pvqz atomic basis is used. The different electronic states of NH are indicated at the right-hand side of (b) and the electronic symmetries for linear HNH are given in the middle part of (b).

is good. The experimental energies are calculated using the thermodynamical data,[26] the calculated zero-point energies of NH(X) (see above) and NH(a) (0.214 eV), and the experimental $NH(a)\leftarrow NH(X)$ transition energy[28] (12 589 cm^{-1}).

Due to the interaction between several states the electronic structure of NH_2 is intricate,[29] especially in the NH +H channel. Cuts through the lowest six PESs for $\alpha=180°$ and 160° are shown in Fig. 3. The calculations are performed in C_s symmetry and the lowest three states of both $^2A''$ and $^2A'$ symmetries are calculated simultaneously. For linearity [Fig. 3(b)] there are two Σ, one Π, and one Δ state; the Π and the Δ states are doubly degenerate. The Π state correlates for small HN–H bond distances with the ground-state minimum and for large HN–H bond distances it correlates with a highly excited state of NH. This leads, for both the $^2A''$ and the $^2A'$ states, to a complicated pattern of avoided crossings for near-linear geometries, as illustrated in Fig. 3(a) for $\alpha=160°$. For the present study, the depletion of $NH(^3\Sigma^-)$, only the lowest $^2A''$ adiabatic state is of relevance.

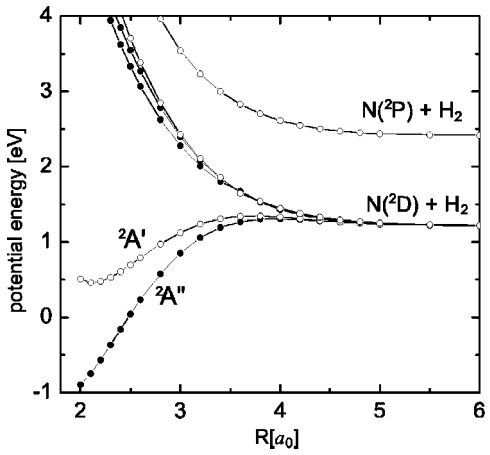

FIG. 4. Cuts through the potential energy surfaces of the lowest six doublet states in the $N+H_2$ channel. R is the distance of N from the center of mass of H_2; the H_2 bond is $r=1.42a_0$ and the angle between **R** and **r** is $\gamma=90°$. The aug-cc-pvqz atomic basis set is used. The energy is normalized such that $E=0$ corresponds to the minimum of the $H(^2S)+NH(X\,^3\Sigma^-)$ channel.

The electronic structure in the $N+H_2$ channel is simpler. In Fig. 4 we show cuts through the six lowest PESs (three $^2A'$ and three $^2A''$ states) as functions of the Jacobi coordinate R. The H_2 bond distance is fixed at $r=1.42a_0$ and the angle is $\gamma=90°$. No avoided crossing complicates the PESs in this asymptotic channel. The lowest two PESs have small barriers, the geometries and energies of which are listed and compared with previous theoretical predictions in Table IV. The barrier of the ground-state PES is slightly lower than the barrier of the excited-state PES. The present results agree well with the previous data of Pederson *et al.*[9,10]

A complication due to a conical intersection occurs, however, at shorter $N-H_2$ bond distances, where the first and the second $^2A'$ states cross each other near the C_{2v} configuration.[29] This is illustrated in Fig. 5 showing potential cuts for the lowest three states with $^2A'$ symmetry, $1\,^2A'$, $2\,^2A'$, and $3\,^2A'$. This figure is the continuation of Fig. 4 to

TABLE IV. Geometries, R and r (in a_0), and energies E (in kcal/mol) for the transition state barriers in the $N+H_2$ channel and several basis sets; $\gamma=90°$.

	$\tilde{X}\,^2A''$			$\tilde{A}\,^2A'$		
Basis	E[a]	R	r	E[a]	R	r
aug-cc-pvtz	2.25	3.926	1.422	3.20	3.722	1.424
	1.93[b]	4.05[b]	1.41[b]	3.39[c]	3.70[c]	1.42[c]
aug-cc-pvqz	2.18	3.936	1.420	3.08	3.740	1.422
aug-cc-pv5z	2.16	3.936	1.419	3.06	3.742	1.421
aug-cc-pv6z	2.16	3.937	1.419	3.05	3.744	1.421

[a]Energies with respect to the $N(^2D)+H_2$ asymptote.
[b]From Table II of Pederson *et al.*, Ref. 9.
[c]From Table I of Pederson *et al.*, Ref. 10.

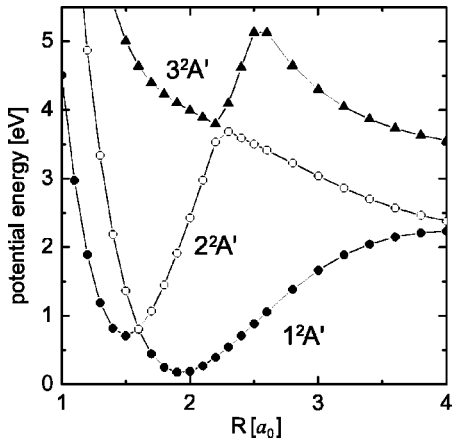

FIG. 5. Cuts through the potential energy surfaces of the three lowest $^2A'$ states in the $N+H_2$ channel. R is the distance of N from the center of mass of H_2; the H_2 bond is $r=2.0a_0$ and the angle between **R** and **r** is $\gamma=90°$. The aug-cc-pvqz atomic basis set is used. The energy is normalized such that $E=0$ corresponds to the minimum of the $H(^2S)+NH(X\,^3\Sigma^-)$ channel. The symbols indicate adiabatic potential energy curves.

smaller bond distances. A (diabatic) state which correlates with a highly excited product channel of $N+H_2$ cuts through all the lower (diabatic) states and thus leads to a series of crossings which become avoided crossings in C_s symmetry. Relevant for our studies of the depletion of NH(X) and NH(a) in collisions with H atoms is only the crossing with

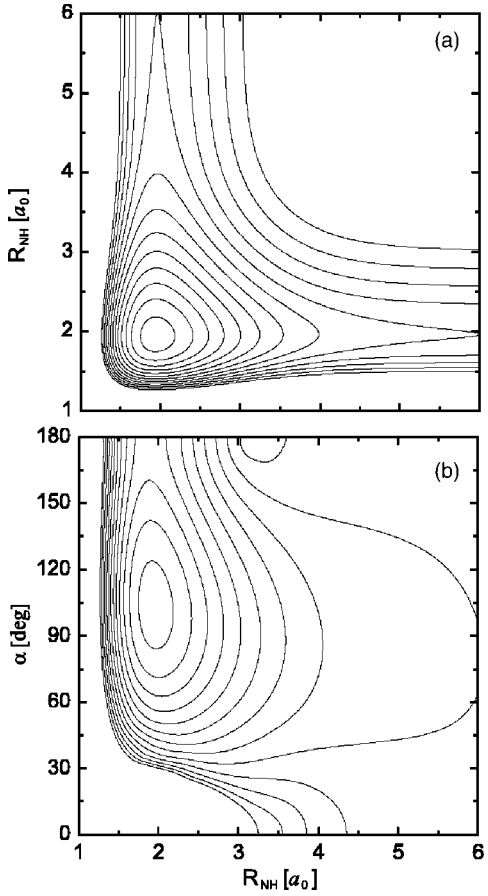

FIG. 6. (a) Contour plot of the $^2A''$ potential energy surface for $\alpha=102.6°$. (b) Contour plot of the $^2A''$ potential energy surface for $R_{NH}=1.94a_0$. The spacing between the contours is 0.5 eV and the highest contour is 2 eV.

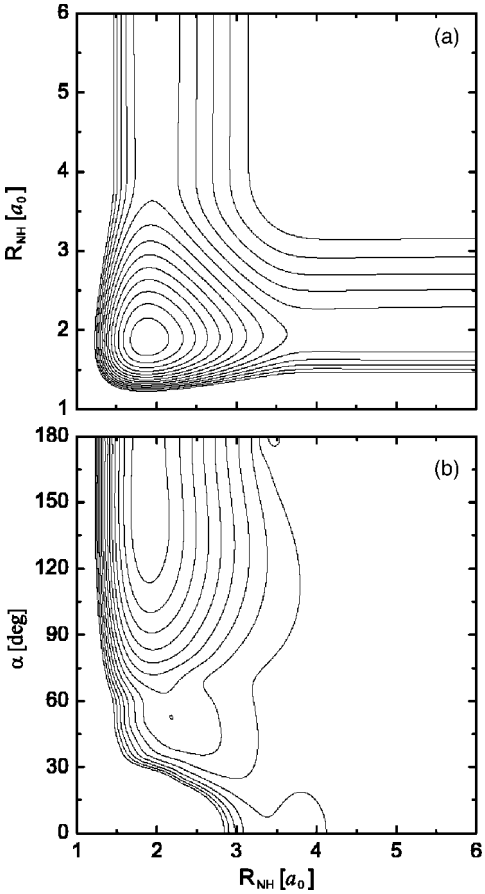

FIG. 7. (a) Contour plot of the $^2A'$ potential energy surface for $\alpha=145.1°$. (b) Contour plot of the $^2A'$ potential energy surface for $R_{NH}=1.88a_0$. The spacing between the contours is 0.5 eV and the highest contour is 4 eV.

the lowest state ($R\approx1.6a_0$), which connects with NH(a) $+H(^2S)$. The location of the crossing depends significantly on r as well as γ. In the construction of the $^2A'$ PES (Sec. III B) we do not explicitly take this avoided crossing into account but merely consider the lowest *adiabatic* state with $^2A'$ symmetry.

B. Construction of potential energy surfaces

The global three-dimensional PESs for the lowest $^2A'$ and the lowest $^2A''$ states are calculated employing the aug-cc-pvqz basis set, which is a reasonable compromise between accuracy and computational cost. Because our primary focus is the reaction of H atoms with NH(X) radicals, we choose the two H–N bond distances R_1 and R_2 and the H–N–H angle α as coordinates for the main three-dimensional grid. Note, these coordinates are different from those used in paper I to calculate the $^4A''$ PES, which has a transition state (TS) at linear N–H–H geometries. The N–H bond lengths (in a_0) are varied between 1.3 and 2.6, 2.8 and 5.0, 5.0 and 6.0, and 7.0 and 9.0 with step sizes of 0.1, 0.2, 0.5, and 1.0, respectively, and α (in degrees) is varied from 0 to 180 with a step size of 10. Additional calculations are performed for 176° for a better description of near-linear geometries. This grid consists of a total of 9424 independent grid points.

The grid defined in the coordinates R_1, R_2, and α, however, is not appropriate for representing the global PES in and near the $N(^4S)+H_2$ channel, that is, in the region of small values of α. Therefore, we define a second grid in terms of the Jacobi coordinates R, r, and γ suitable for the $N+H_2$ channel. R (in a_0) is varied from 1.8 to 2.6, 2.8 to 5.0, 5.0 to 5.5, and 6.0 to 9.0 with step sizes of 0.1, 0.2, 0.5, and 1.0, respectively. The H_2 bond length (in a_0) is varied between 0.9 and 2.2 and 2.4 and 3.0 with step lengths of 0.1 and 0.2, and the Jacobi angle γ is varied from 10 to 90° with a step size of 10°; additional calculations are performed at 2°. The second grid comprises a total of 4680 points.

Analytical representations for both PESs and both grids are obtained separately by three-dimensional cubic spline interpolation. If V_1 and V_2 denote the two potential representations on the bond-coordinate and the Jacobi-coordinate grids, respectively, combined potentials are constructed by

$$V=\begin{cases} V_1 & \text{for } r \geqslant 3a_0 \\ V_1 f + V_2(1-f) & \text{for } r \leqslant 3a_0, \end{cases} \tag{5}$$

where $f=\exp[-5(r-3)^2]$. Equation (5) applies to both the $^2A'$ and the $^2A''$ PESs.

Contour plots of the $^2A''$ PES are shown in Fig. 6. The $^2A''$ PES is purely attractive at large HN–H distances and the TS region towards linearity is wide as one can see in Fig. 6(b). Similar plots are depicted in Fig. 7 for the $^2A'$ PES. Because of the conical intersection of the $^2A'$ state with the second state of the same symmetry at small angles α, a shallow second minimum is seen near $\alpha=50°$ in Fig. 7(b). The main minimum is very shallow toward the linear H–N–H geometry; the barrier to linearity on the $^2A'$ PES is only 1.981 kcal/mol. For long HN–H distances the ground-state PES is more attractive than the excited-state PES, as demonstrated in Fig. 8, where we show the energies along the minimum-energy paths for both states. The different attractions of both PESs will have consequences for the corresponding reaction cross sections.

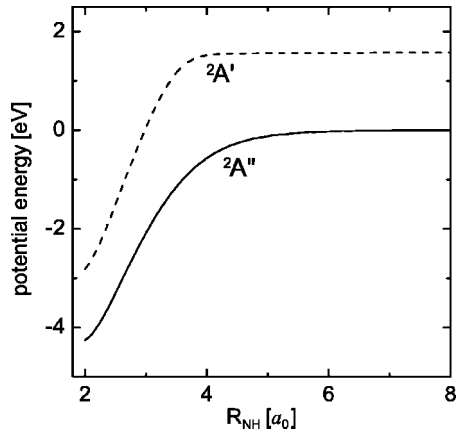

FIG. 8. Potential energy in the H+NH channel along the minimum-energy path for the lowest $^1A''$ and $^1A'$ states. The other N–H bond length and the bond angle α are optimized.

C. Calculation of bound states

In order to assess the accuracy of the ground-state PES—apart from equilibrium geometries and dissociation energies—we calculate the low-lying vibrational energies for total nuclear angular momentum $J=0$ and compare them with the experimental transition energies. A complete theoretical description should take into account the electronic angular momentum, i.e., the RT coupling between the $^2A''$ and $^2A'$ states. Such calculations have been performed for NH_2 by, for example, Gabriel *et al.*[7] These authors have used *ab initio* PESs, which were modified, however, by a least-squares procedure to reproduce the experimental data with

TABLE V. Comparison of calculated and measured vibrational transition energies for $NH_2(\tilde{X})$ and $J=0$.

i	(v_1,v_2,v_3)	E	Expt.−calc.[a]	i	(v_1,v_2,v_3)	E	Expt.− calc.
1	0,0,0	0	0	21	0,6,0	8439.0	12.5
2	0,1,0	1497.1	0.2	22	1,4,0	8929.9	12.7
3	0,2,0	2960.8	0.4	23	0,4,1	9007.4	⋯
4	1,0,0	3209.5	9.9	24	2,2,0	9206.3	20.9
5	0,0,1	3288.3	12.8	25	1,2,1	9230.7	⋯
6	0,3,0	4390.1	1.2	26	3,0,0	9289.1	⋯
7	1,1,0	4694.1	⋯	27	2,0,1	9300.4	⋯
8	0,1,1	4766.3	⋯	28	0,2,2	9403.0	18.5
9	0,4,0	5783.4	2.2	29	1,0,2	9525.8	⋯
10	1,2,0	6141.0	10.9	30	0,0,3	9653.1	⋯
11	0,2,1	6211.1	⋯	31	0,7,0	9673.7	43.2
12	2,0,0	6315.1	⋯	32	1,5,0	10 266.1	20.2
13	1,0,1	6350.3	⋯	33	0,5,1	10 354.3	⋯
14	0,0,2	6518.1	⋯	34	2,3,0	10 600.7	8.3
15	0,5,0	7136.1	4.3	35	1,3,1	10 626.1	⋯
16	1,3,0	7553.4	11.2	36	3,1,0	10 737.6	⋯
17	0,3,1	7625.3	⋯	37	2,1,1	10 747.9	⋯
18	2,1,0	7785.2	19.3	38	0,3,2	10 799.5	⋯
19	1,1,1	7814.9	⋯	39	0,8,0	10 814.9	133.1
20	0,1,2	7977.6	22.8	40	1,1,2	10 978.1	⋯

[a]Experimental transition energies taken from Table 6 in Ref. 7.

TABLE VI. Calculated rate coefficients (in $cm^3\,mol^{-1}\,s^{-1}$) as functions of temperature.

	$NH(X\,^3\Sigma^-)+D(^2S)\rightarrow$		$ND(X\,^3\Sigma^-)+H(^2S)\rightarrow$	
	$ND(X\,^3\Sigma^-)$	$N(^4S)$	$NH(X\,^3\Sigma^-)$	$N(^4S)$
T	$+H(^2S)$	$+HD(X\,^1\Sigma_g^+)$	$+D(^2S)$	$+HD(X\,^1\Sigma_g^+)$
250	3.7(13)[a]	6.4 (11)	2.8 (13)	2.2 (11)
300	4.0 (13)	9.1 (11)	3.0 (13)	3.7 (11)
350	4.1 (13)	1.2 (12)	3.1 (13)	5.5 (11)
400	4.3 (13)	1.6 (12)	3.2 (13)	7.6 (11)
500	4.5 (13)	2.3 (12)	3.4 (13)	1.3 (12)
700	4.7 (13)	4.0 (12)	3.7 (13)	2.5 (12)
900	4.8 (13)	5.8 (12)	3.8 (13)	3.9 (12)

[a]Numbers in parentheses indicate powers of ten.

high precision. A complete description of the spectroscopy of NH_2 is beyond the purpose of the present investigation. Here, we consider only the low-lying vibrational states of the $^2A''$ electronic state, and particularly those with modest excitation of the bending degree of freedom. The states which are well below the minimum of the $^2A'$ PES are not affected by the coupling. Even if the excitation energy is above the bottom of the $^2A'$-state PES, the effect of RT coupling is expected to be small, provided that the bending degree is only weakly excited. In such cases the wave functions do not extend much to linear geometries where the RT coupling is localized.

The calculations of the bound states are performed using the Jacobi coordinates appropriate for the NH–H channel: R', the distance from H to the center of mass of NH; r', the NH bond length; and γ', the vector between the vectors $\mathbf{R}'$ and $\mathbf{r}'$. Note, these Jacobi coordinates are different from the ones used above for describing the $N+H_2$ channel. The filter diagonalization method[30,31] is used to determine the vibrational energy levels and wave functions. The Hamiltonian is evaluated by a three-dimensional discrete variable representation (DVR).[32] The DVR grid in R' ranges from 1.4 to $4.0a_0$ with 80 grid points, the grid in r' ranges from 0.9 to $4.0a_0$ also with 80 DVR points, and γ' is varied between 0 and 180° with 160 Gauss Legendre points. Points on this grid with an energy of 3.5 eV above the minimum are discarded.

The first 40 vibrational transition energies for the $^2A''$ state are listed in Table V and compared with experimental data, as given in Table VI of Ref. 7. The agreement is very good, except for the high bending states (0,7,0) and (0,8,0). The latter two states lie well above the barrier for linearity (1.46 eV above equilibrium) and therefore a model without RT coupling is not appropriate.

A similar study for the excited state without RT coupling to the ground state is not meaningful. Therefore, only a harmonic analysis is performed in the minimum of the $^2A'$ PES. The three harmonic frequencies (in cm^{-1}) are 977.6 (964), 3619.2 (3635), and 3931.3 (3953). They agree well with the harmonic frequencies for the $^2A'$ state of Gabriel *et al.*[7] (values in parentheses), which have been fitted to reproduce the experimental transition energies. In summary, both PESs are of high quality.

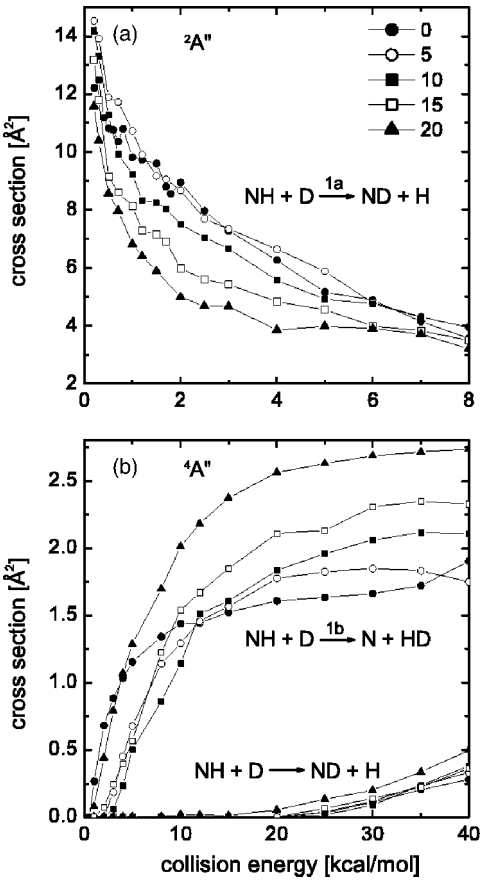

FIG. 9. (a) Cross sections for reaction (1a) as function of the collision energy E_c and the initial rotational quantum number j of NH as indicated. Calculated using the $^2A''$ potential energy surface of this work. (b) Cross sections for reaction (1b) as function of E_c and j, calculated using the $^4A''$ potential energy surface of Ref. 3. The lower part shows the cross sections for the exchange reaction on the $^4A''$ potential energy surface.

IV. TRAJECTORY CALCULATIONS

Cross sections for reactions (1a) and (1b) are calculated by classical trajectories as functions of the collision energy E_c and the initial rotational state j of $NH(X\,^3\Sigma^-)$.[33] Since temperatures only up to about 1000 K are considered, the initial vibrational state is $\nu=0$ throughout the present investigation. The collision energy is varied up to 15 kcal/mol for reaction (1a) and up to 40 kcal/mol for reaction (1b). The initial rotational state is varied up to $j=20$ in both cases. The internal energy of NH is initially set to the quantum-mechanical zero-point energy for a particular state $(\nu=0,j)$. The maximum impact parameter is separately adjusted for each collision energy. For each E_c and j, typically 10 000 trajectories are calculated.

The results of the cross-section calculations are depicted in Fig. 9. The cross sections for reaction (1b) are, of course, very similar to the results in paper I for the reaction $NH(X\,^3\Sigma^-)+H(^2S)\rightarrow N(^4S)+H_2(X\,^1\Sigma_g^+)$. Because there is a barrier in the reactant channel, the cross sections show a pronounced threshold behavior and a sizable j dependence. However, for a given E_c and j the cross sections for D as collision partner are larger than for H atoms colliding with NH (see Fig. 5 in paper I). A possible reason is that, because of the smaller relative velocity for NH+D, the reactants are

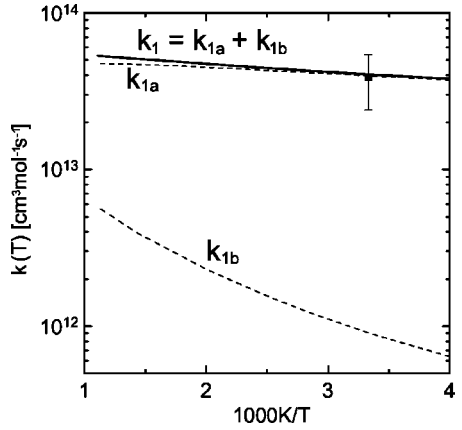

FIG. 10. Calculated (solid and dashed lines) and experimental (■) rate coefficients as function of temperature for reactions (1), (1a), and (1b).

more effectively funneled through the narrow TS near linear N–H–D, respectively, N–H–H arrangements. The cross sections for the isotope exchange reaction (1a) proceeding on the $^4A''$ PES [lower part of Fig. 9(b)] are much smaller than the cross sections for reaction (1b); they are of no importance for the depletion of NH($X\,^3\Sigma^-$) and are not taken into account in the subsequent calculation of the rate coefficients.

The cross sections for reaction (1a) [Fig. 9(a)] monotonously decrease with the collision energy as it is expected for a wide TS with no barrier. In the intermediate energy regime the cross sections show a clear-cut j dependence, i.e., initial rotation gradually decreases the reactivity. For very low and for higher energies this dependence is not so clear.

Temperature-dependent rate coefficients are calculated by

$$k(T) = \frac{\eta}{(\pi\mu)^{1/2}}\left(\frac{2}{k_B T}\right)^{3/2} Q^{-1}\sum_j (2j+1)\exp(-E_{\nu j}/k_B T) \times \int_0^\infty E_c \sigma(E_c,\nu,j)\exp(-E_c/k_B T)dE_c, \quad (6)$$

where μ is the reduced mass for the reactant channel, k_B is the Boltzmann constant, Q is the vibrational-rotational partition function, and $E_{\nu j}$ is the energy of NH(X) in state ($\nu=0, j$). The electronic degeneracy factor η is taken as $1/3$ and $2/3$ for reactions (1a) and (1b), respectively. These degeneracy factors reflect the spin multiplicities of the $^2A''$ and $^4A''$ states via which reactions (1a) and (1b) proceed.

Rate coefficients for reactions (1a) and (1b) are calculated in the range 250–1000 K (Fig. 10 and Table VI). k_{1a} is of the order of $(4–5)\times10^{13}$ cm^3 mol^{-1} s^{-1} and shows a very small positive temperature dependence. The rate coefficient for reaction (1b), on the other hand, is much smaller and therefore the total rate coefficient $k_1=k_{1a}+k_{1b}$ is mainly determined by k_{1a}. Because of its strong positive temperature dependence, however, the relative contribution of k_{1b} slightly increases with temperature. Interestingly, the rate coefficient for reaction (1b) is roughly the same as the rate coefficient for the reaction NH($X\,^3\Sigma^-$)+H(^2S)→N(^4S)+H$_2$($X\,^1\Sigma_g^+$) calculated in paper I. The decrease of the prefactor due to $\mu^{-1/2}$ in Eq. (6) by a factor of approximately 0.7 for D atoms is compensated by an increase of the reaction cross sections as discussed above.

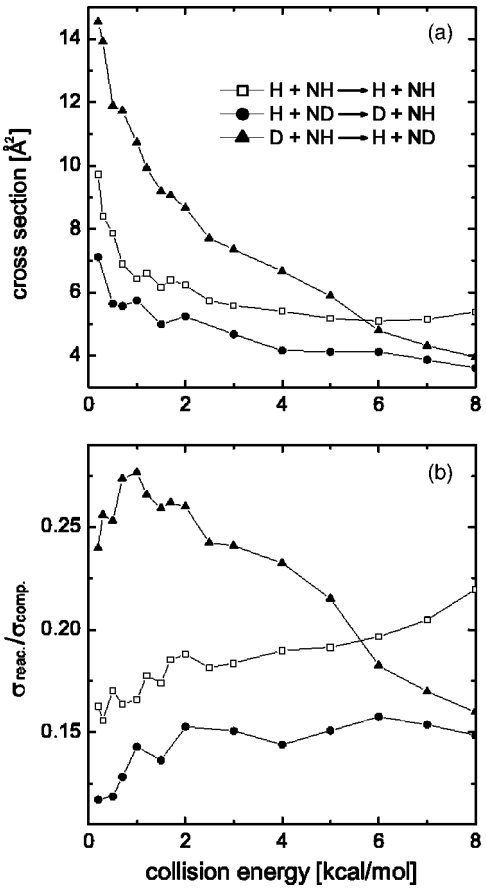

FIG. 11. (a) Cross sections for the exchange reaction on the $^2A''$ potential energy surface for three different isotope combinations as indicated. The initial rotational state of the diatom is $j=5$. (b) Ratio of the reaction and the complex formation cross section for the three isotope combinations indicated in (a).

The calculated rate coefficient at room temperature for reaction (1) is $k_1=4.1\times10^{13}$ cm^3 mol^{-1} s^{-1}. It is in very good agreement with the measured value of $k_1=(3.9\pm1.5)\times10^{13}$ cm^3 mol^{-1} s^{-1}.

In order to get a better understanding of the dynamics of reaction (1a) we calculate not only the cross section for the isotope exchange reaction (σ_{reac}) but also the cross section for the formation of a $NH_2(\tilde{X})^{\ddagger}$ complex (σ_{comp}). When D and NH approach each other on the $X\,^2A''$-state PES they experience a strong attraction and first form a highly excited complex. We define that a complex is created when the potential energy along a trajectory falls below a certain value $\overline{V}(\tilde{X})$; in the present application we choose $\overline{V}(\tilde{X})=-1.25$ eV (which is 3 eV above the potential minimum). If energy were completely randomized among all degrees of freedom, one would expect that the complex breaks apart into the two identical product channels NH+D and ND+H with equal probability. The consequence would be that the reaction cross section σ_{reac} is approximately half the complex formation cross section σ_{comp} This is, however, not the case as illustrated in Fig. 11(b). The ratio $P=\sigma_{reac}/\sigma_{comp}$ is significantly smaller than 0.5 for all the three possible isotope com-

binations shown in Fig. 11(b): H+NH, D+NH, and H+ND. The $NH_2(\tilde{X})^{\ddagger}$, respectively, $NHD(\tilde{X})^{\ddagger}$ complex preferentially breaks apart into the educt channel, i.e., the memory on the entrance channel is not washed out during the lifetime of the complex. In many trajectories the impinging atom enters the complex, is rapidly accelerated by the deep potential well, hits the NH radical, and quickly leaves the complex in the entrance channel; it does not have much time for energy redistribution. With other words, although the potential well is more than 4 eV deep, the reactions of D atoms with $NH(X)$ radicals on the ground-state PES are not statistical. This is also underlined by the observation that the lifetimes for the reactive trajectories $[D+NH \rightarrow (NHD)^{\ddagger} \rightarrow H+ND]$ are about a factor of 2.5 longer than for the nonreactive trajectories $[D+NH \rightarrow (NHD)^{\ddagger} \rightarrow D+NH]$.

The nonstatistical effect depends markedly on the isotope combination and therefore on the reduced masses μ of the reactant and product channels ($\mu \approx m_H$ or $\mu \approx m_D$ depending on whether the atom is H or D, respectively). It is largest for the reaction $H+ND \rightarrow NH+D$ and smallest for the reaction $D+NH \rightarrow ND+H$. Apparently, the light H atom is directly repelled from the inner core of the PES more effectively than the twice as heavy D atom. The $D+NH \rightarrow ND+H$ reaction is more statistical at low collision energies but becomes more direct with increasing energy. The other two reactions show a different energy dependence for P, i.e., the statistical behavior slightly increase with E_c, at least for the range of E_c shown in Fig. 11(b). The isotope dependence of P leads to an isotope dependence of the reaction cross section [Fig. 11(a)]. σ_{reac} is largest for D+NH and it is smallest for H+ND. The cross section for the formation of a collision complex is practically the same for all three isotope combinations.

We have calculated also the rate coefficients for the reactions $ND(X\,^3\Sigma^-)+H(^2S) \xrightarrow{k'_{1a}} NH(X\,^3\Sigma^-)+D(^2S)$ and $ND(X\,^3\Sigma^-)+H(^2S) \xrightarrow{k'_{1b}} N(^4S)+HD(X\,^1\Sigma_g^+)$, that is, reactions (1a) and (1b) but with H and D interchanged. The results are given in Table VI. Because of the isotope dependence of the nonstatistical behavior described above, the rate coefficient $k'_{1a}+k'_{1b}$ is smaller than $k_{1a}+k_{1b}$ despite the increase of the kinetic factor $\mu^{-1/2}$ by approximately 1.4 in the rate expression for the reactions $H+ND(X)$.

V. CONCLUSIONS

We have measured, for the first time, the consumption of $NH(X)$ radicals in reactions with D atoms, i.e., $NH(X)+D(^2S) \rightarrow$ products (1). The measured rate coefficient at room temperature is $k_1=(3.9\pm1.5)\times10^{13}$ cm^3 mol^{-1} s^{-1}. Comparing this value with the rate coefficient obtained for $NH(X)+H(^2S) \rightarrow$ products (2) it can be concluded that reaction (1) is mainly determined by the H/D exchange reaction, which has to occur on the $^2A''$ ground state potential energy surface (PES). The other possible reaction channel, i.e., the production of $N(^4S)$ atoms, is significantly slower as observed experimentally in reaction (2). From the ratio of the reaction paths in reaction (1) leading to the depletion of $NH(X)$ or recovery of $NH(X)$, which is obtained from the trajectory calculations, it can be concluded that the high-pressure limit of the rate coefficient of reaction (1) is of the order of $k_1(\infty)=1.6\times10^{14}$ cm^3 mol^{-1} s^{-1}.

The experimental data of the equilibrium geometries, dissociation energies, and the $^2A''/^2A'$ separation are well described by the two global PESs for the $^2A''$ and $^2A'$ states of NH_2 constructed by *ab initio* calculations (MRCI, full-valence CASSCF wave functions, and aug-cc-pvqz basis set). Furthermore, the calculated vibrational transition energies in the electronic ground state are in very good agreement with the experimental energies.

Cross sections for reactions (1a) and (1b) have been calculated by classical trajectories over wide ranges of the collision energy and the initial rotational state. In accordance with a barrierless PES and a wide transition state, the reaction cross section for the $^2A''$ state decreases with increasing collision energy. In contrast, the cross section for reactions proceeding on the $^4A''$ PES increases with energy, in agreement with a reaction barrier and a linear transition state.

The calculated rate coefficient for reaction (1) is in good agreement with the measured one. The contribution of reaction (1b) at room temperature is only 2%. The good agreement with the measured rate coefficient indicates that Renner–Tenner coupling between the $^2A''$ and $^2A'$ states is unimportant for reaction (1).

Despite the more than 4 eV deep potential well of the $^2A''$ PES, the reaction dynamics is not statistical. The temporarily formed $NH_2(\tilde{X})^{\ddagger}$ complex preferentially decays to the educts channel, i.e., energy redistribution is far from complete. The nonstatistical effect depends markedly on the isotope constitution. It is largest for H+ND and smallest for D+NH. The strong isotope dependence leads to a reduction of the rate coefficient for the reaction $H+ND(X) \rightarrow$ products.

ACKNOWLEDGMENTS

The authors are grateful to Professor J. Troe for stimulating interest and financial support. They also thank Professor P. Rosmus for performing the harmonic analysis for the $^2A'$ potential energy surface. Financial support from the Fonds der Chemischen Industrie is acknowledged.

[1] B. S. Haynes, Combust. Flame **28**, 81 (1977).
[2] B. S. Haynes, Combust. Flame **28**, 113 (1977).
[3] L. Adam, W. Hack, H. Zhu, Z.-W. Qu, and R. Schinke, J. Chem. Phys. **122**, 11430 (2005).
[4] W. Hack and A. Wilms, J. Phys. Chem. **93**, 3540 (1989).
[5] R. J. Buenker, M. Peric, S. D. Peyerimhoff, and R. Marian, Mol. Phys. **43**, 987 (1981).
[6] R. N. Dixon, S. J. Irving, J. R. Nightingale, and M. Vervloet, J. Chem. Soc., Faraday Trans. **87**, 2121 (1991).
[7] W. Gabriel, G. Chambaud, P. Rosmus, S. Carter, and N. C. Handy, Mol. Phys. **81**, 1445 (1994).
[8] Work in progress.
[9] L. A. Pederson, G. C. Schatz, T.-S. Ho, T. Hollebeek, H. Rabitz, L. B. Harding, and G. Lendvay, J. Chem. Phys. **110**, 9091 (1999).
[10] L. A. Pederson, G. C. Schatz, T. Hollebeek, T.-S. Ho, H. Rabitz, and L. B. Harding, J. Phys. Chem. A **104**, 2301 (2000).
[11] T.-S. Ho, H. Rabitz, F. J. Aoiz, L. Bañares, S. A. Vázquez, and L. B. Harding, J. Chem. Phys. **119**, 3063 (2003).
[12] M. Alagia, N. Balucani, L. Cartechini *et al.*, J. Chem. Phys. **110**, 8857 (1999).
[13] F. Santoro, C. Petrongolo, and G. C. Schatz, J. Phys. Chem. A **106**, 8276

(2002).
[14]P. Honvault and J.-M. Launay, J. Chem. Phys. **111**, 6665 (1999).
[15]P. Honvault and J.-M. Launay, Chem. Phys. Lett. **329**, 233 (2000).
[16]N. Balucani, L. Cartechini, G. Capozza *et al.*, Phys. Rev. Lett. **89**, 013201 (2002).
[17]H.-J. Werner and P. J. Knowles, J. Chem. Phys. **89**, 5803 (1988).
[18]P. J. Knowles and H.-J. Werner, Chem. Phys. Lett. **145**, 514 (1988).
[19]S. R. Langhoff and E. R. Davidson, Int. J. Quantum Chem. **8**, 61 (1974).
[20]H.-J. Werner and P. J. Knowles, J. Chem. Phys. **82**, 5053 (1985).
[21]P. J. Knowles and H.-J. Werner, Chem. Phys. Lett. **115**, 259 (1985).
[22]T. H. Dunning, Jr., J. Chem. Phys. **90**, 1007 (1989).
[23]H.-J. Werner, P. J. Knowles, R. Lindh *et al.*, MOLPRO, version 2002.6, a package of ab initio programs (2003); see http://www.molpro.net
[24]I. Morino and K. Kawaguchi, J. Mol. Spectrosc. **182**, 428 (1997).
[25]G. Herzberg, *Electronic Spectra and Electronic Structure of Polyatomic Molecules*, Molecular Spectra and Molecular Structure Vol. III (Van Nostrand, Princeton, 1966).
[26]The thermodynamical data for ΔH (in kcal/mol) from Ref. 27 are 84.0 for NH, 52.1 for H, 112.9 for N, 0.0 for H_2, and 44.19 for NH_2.
[27]*CRC Handbook of Chemistry and Physics*, 83th Ed., edited by D. R. Lide (CRC Boca Raton, 2002).
[28]NIST Standard Reference Data Bank, http://webbook.nist.gov/.
[29]T. Takayanagi, Y. Kurosaki, and K. Yokoyama, Chem. Phys. Lett. **321**, 106 (2000).
[30]V. A. Mandelshtam and H. S. Taylor, J. Chem. Phys. **102**, 7390 (1995).
[31]T. P. Grozdanov, V. A. Mandelshtam, and H. S. Taylor, J. Chem. Phys. **103**, 7990 (1995).
[32]J. C. Light and T. Carrington, Adv. Chem. Phys. **114**, 263 (2000).
[33]M. Karplus, R. N. Porter, and R. D. Sharma, J. Chem. Phys. **43**, 3259 (1965).